Streamflow and satellite evapotranspiration are asymmetric calibration targets in water-limited catchments

Roland Yonaba[1,*], Tazen Fowé[1], Soumahila Sankandé[1], Nazira Tinto[1], Omar Goudiaby[2], Elias Nkiaka[3], Arsène Kiéma[4], Ansoumana Bodian[2], Harouna Karambiri[1]

[1]Laboratoire Eaux, Hydro-Systèmes et Agriculture (LEHSA), Institut International d'Ingénierie de l'Eau et de l'Environnement (2iE), 01 BP 594, Ouagadougou, Burkina Faso
[2]Laboratoire Dynamique des Territoires et Développement (Leïdi), Université Gaston Berger (UGB), BP 2, Saint-Louis, Sénégal.
[3]Climate, Catchments, Coasts and Community Research Group, School of Natural Sciences, University of Lincoln, Lincoln, UK
[4]Département Climat-Eau-Sol, Centre Climatique Régional pour l'Afrique de l'Ouest et du Sahel (CCR-AOS), BP 11011, Niamey, Niger

Correspondence to: Roland Yonaba (ousmane.yonaba@2ie-edu.org)

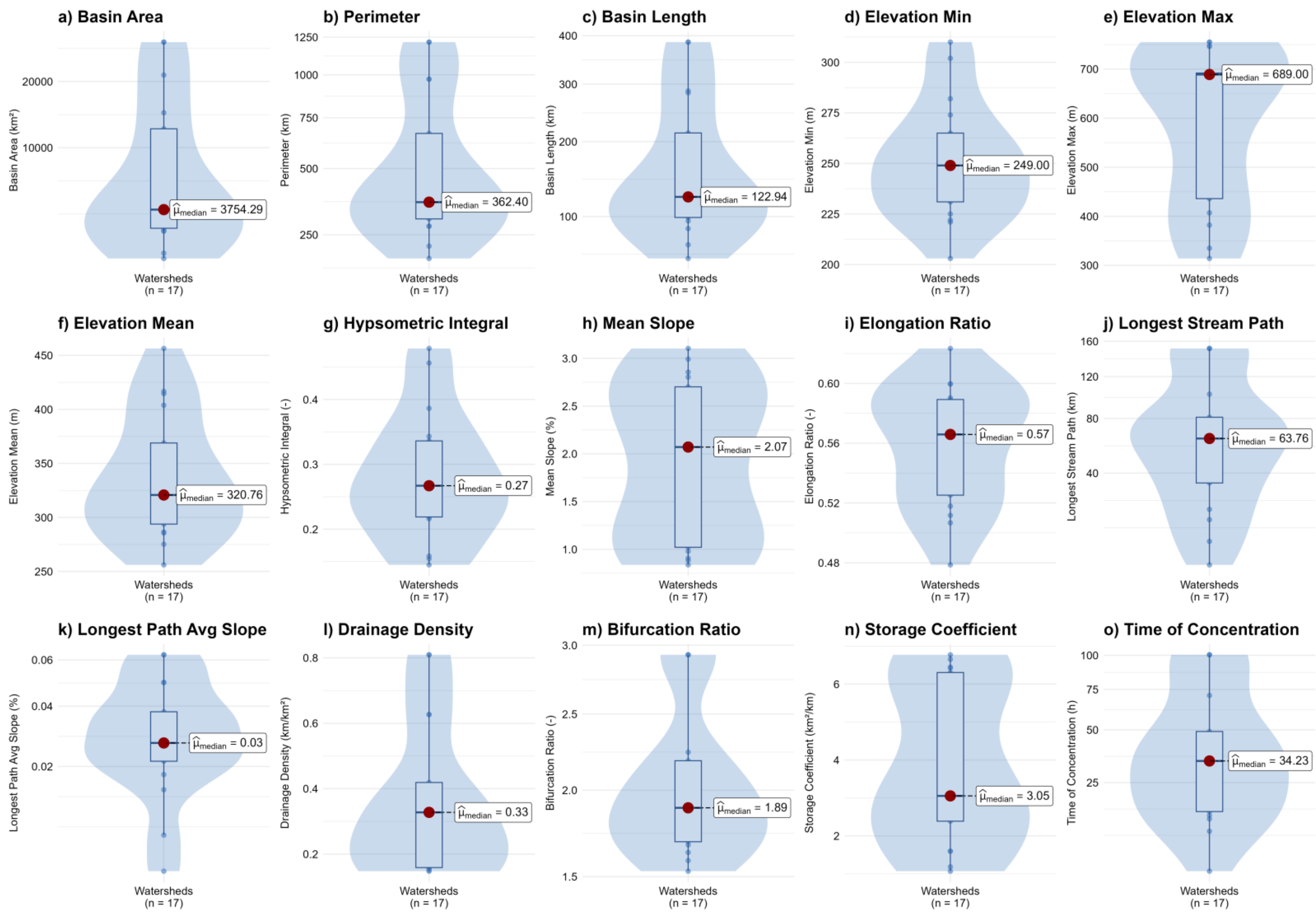

Figure S1: Distribution of morphometric characteristics of the study watersheds, derived from the HydroSHEDS v1 digital elevation model (Lehner et al., 2008): (a) basin area, (b) perimeter, (c) basin length, (d) minimum elevation, (e) maximum elevation, (f) mean elevation, (g) hypsometric integral, (h) mean slope, (i) elongation ratio, (j) longest stream path, (k) average slope along the longest flow path, (l) drainage density, (m) bifurcation ratio, (n) storage coefficient, and (o) time of concentration (Kirpich method). The red points in the box plots and labels give the median value.

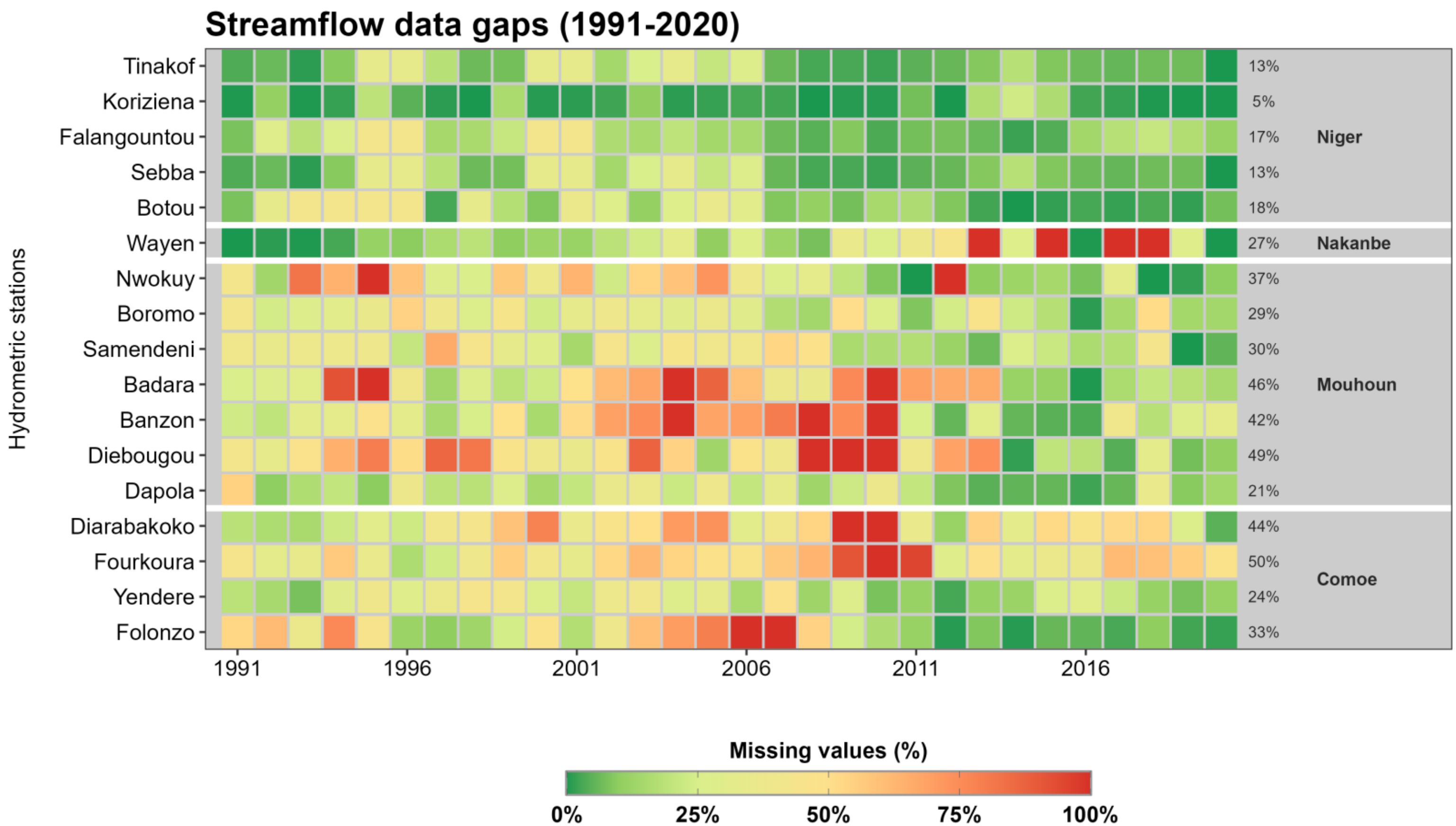

Figure S2: Annual missing-data rate (%) for daily streamflow at the 17 gauging stations over the period 1991-2020, grouped by river basin (Niger, Nakanbe, Mouhoun, Comoé).

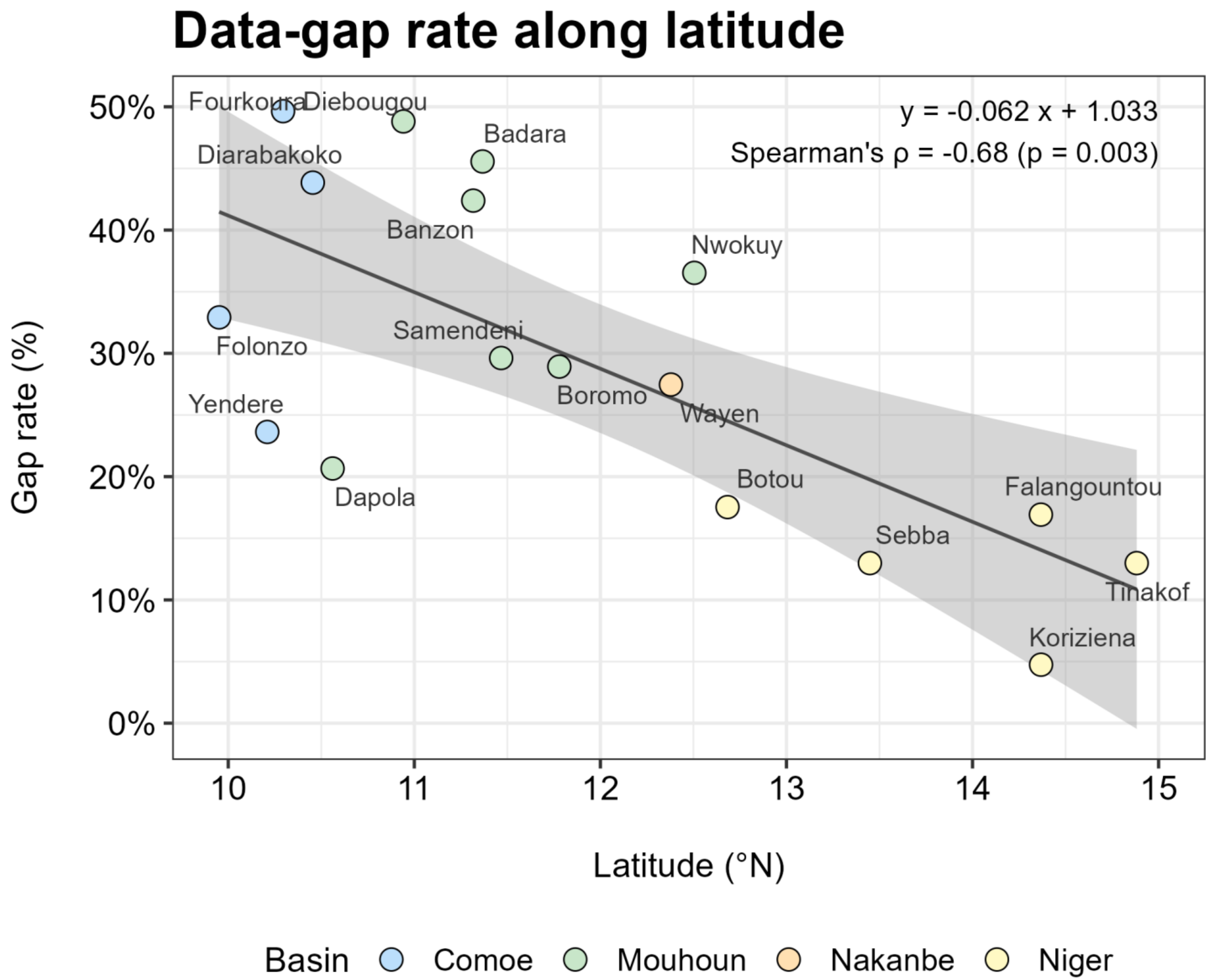

Figure S3: Station data-gap rate (1991-2020) as a function of latitude across the 17 retained gauging stations. Each point is a station, coloured by river basin (Comoe, Mouhoun, Nakanbe, Niger); the solid line is the ordinary least-squares fit with its 95% confidence band in grey shade. Gap rate decreases significantly with latitude (Spearman's ρ = -0.68, p = 0.003), with the most complete records concentrated among the semi-arid northern stations.

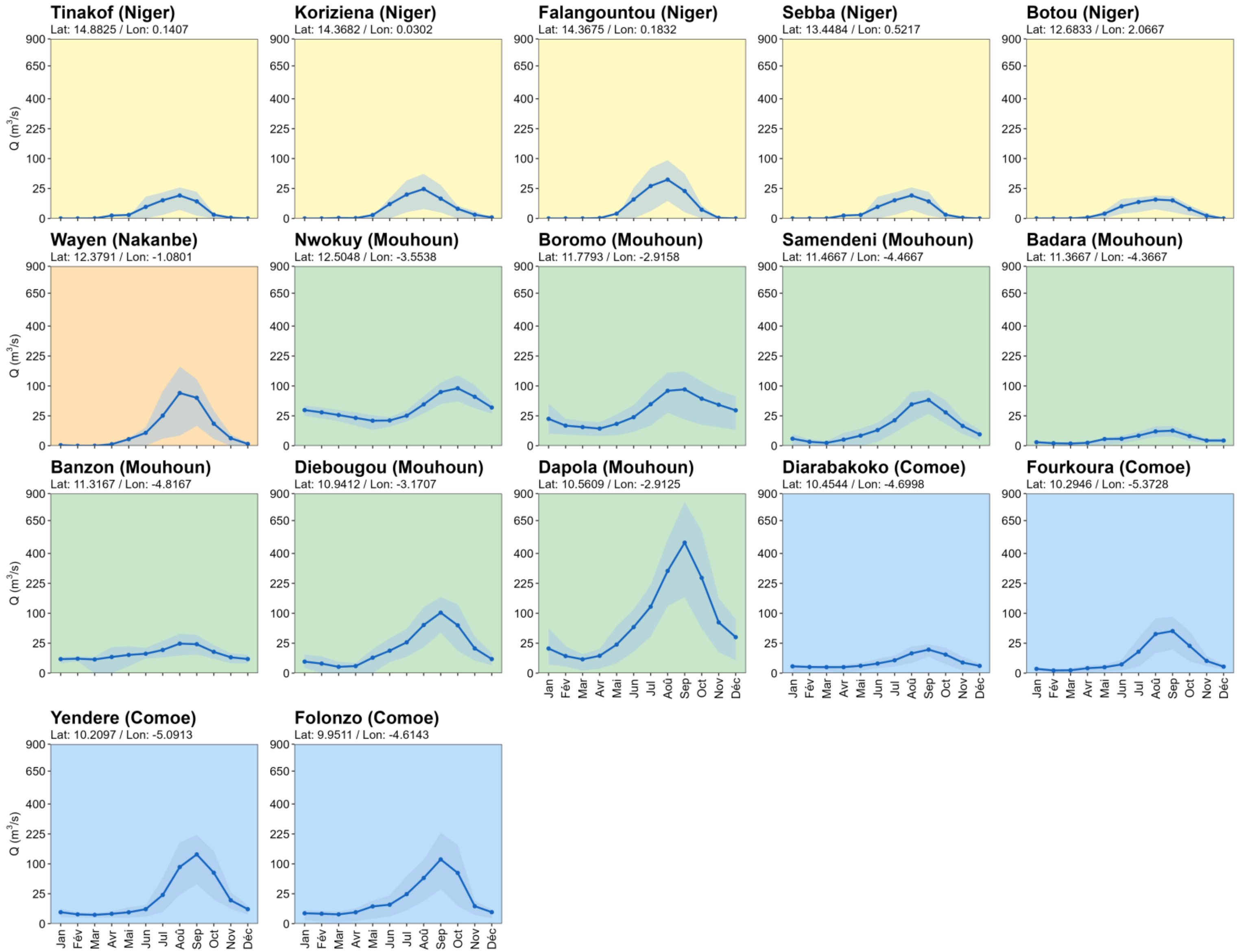

Figure S4: Mean monthly discharge regime (1991-2020) at the 17 gauging stations, ordered by basin (Niger, Nakanbe, Mouhoun, Comoé). Solid line is the multi-year monthly mean and shaded band is the 5th-95th quantile range.

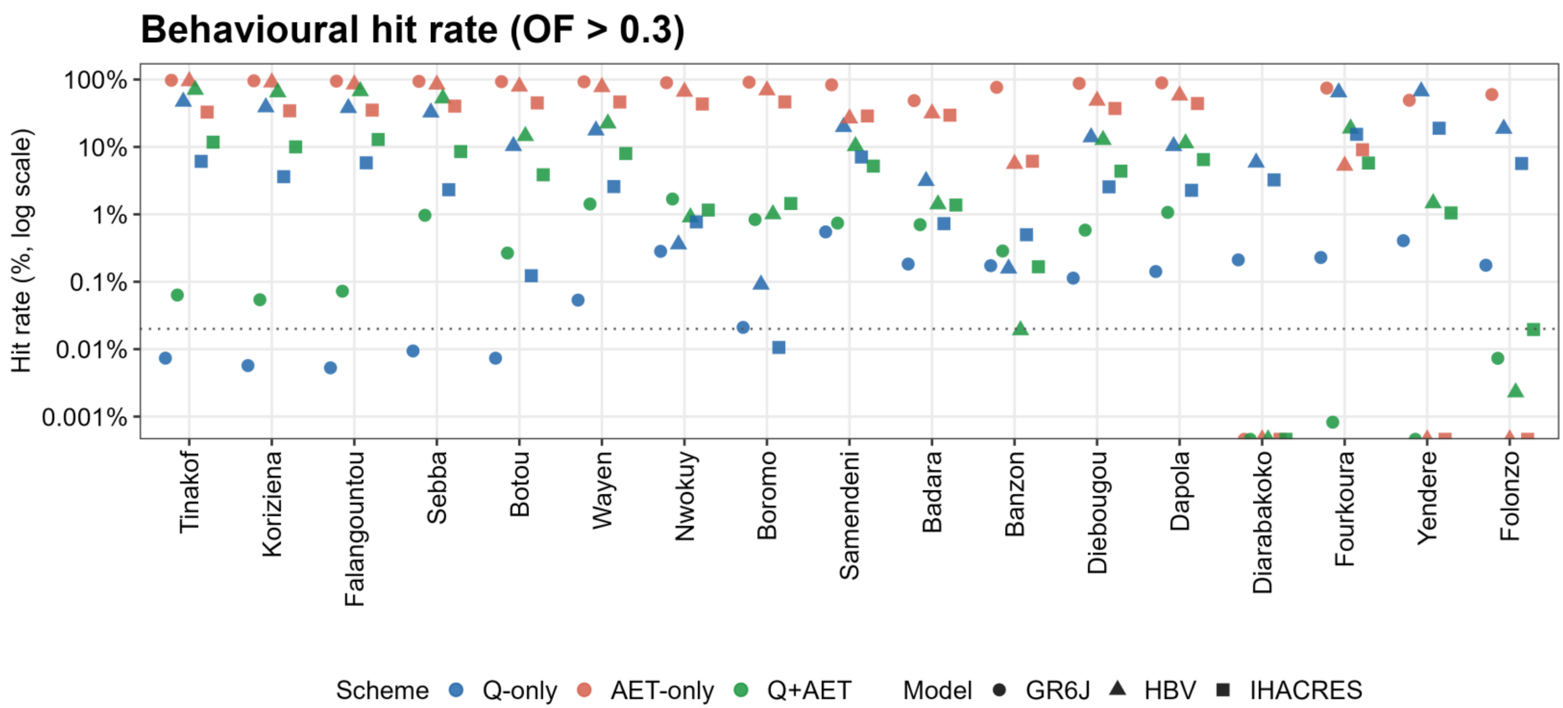

Figure S5: Behavioural hit rate (percentage of the 250,000-member prior sample retaining OF > 0.3) for each of the 17 watersheds, by calibration scheme and model. Hit rate is shown on a log scale. The dotted horizontal line marks the hit rate corresponding to 50 behavioural sets (n_post = 50), the minimum retained for the permutation-based constraint analysis. Points falling below this line indicate model-scheme-watershed combinations excluded as unidentifiable.

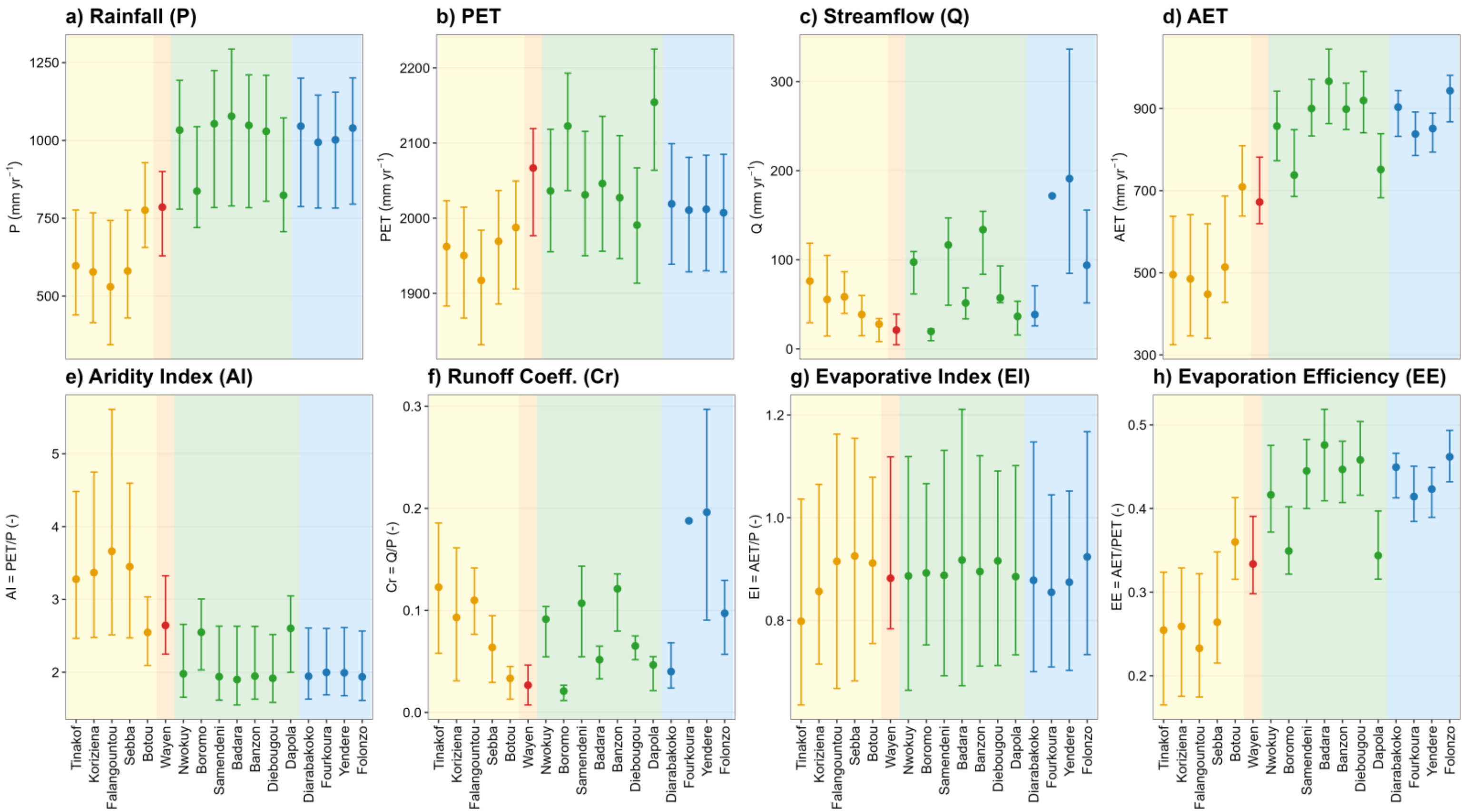

Figure S6: Long-term (1991-2020) annual water-balance components and derived indices for the 17 watersheds, ordered from north (left) to south (right) and coloured by basin (Niger: pale yellow; Nakanbe: pale orange; Mouhoun: pale green; Comoé: pale blue). (a) Mean annual precipitation (P); (b) Synoptic station potential evapotranspiration (PET); (c) streamflow (Q); (d) actual evapotranspiration (AET, GLEAM v4.3a); (e) aridity index (AI = PET/P); (f) runoff coefficient (Cr = Q/P); (g) evaporative index (EI = AET/P); (h) evaporation efficiency (EE = AET/PET). Points show the long-term mean; error bars show the 5th -95th percentile range of annual values over 1991-2020.

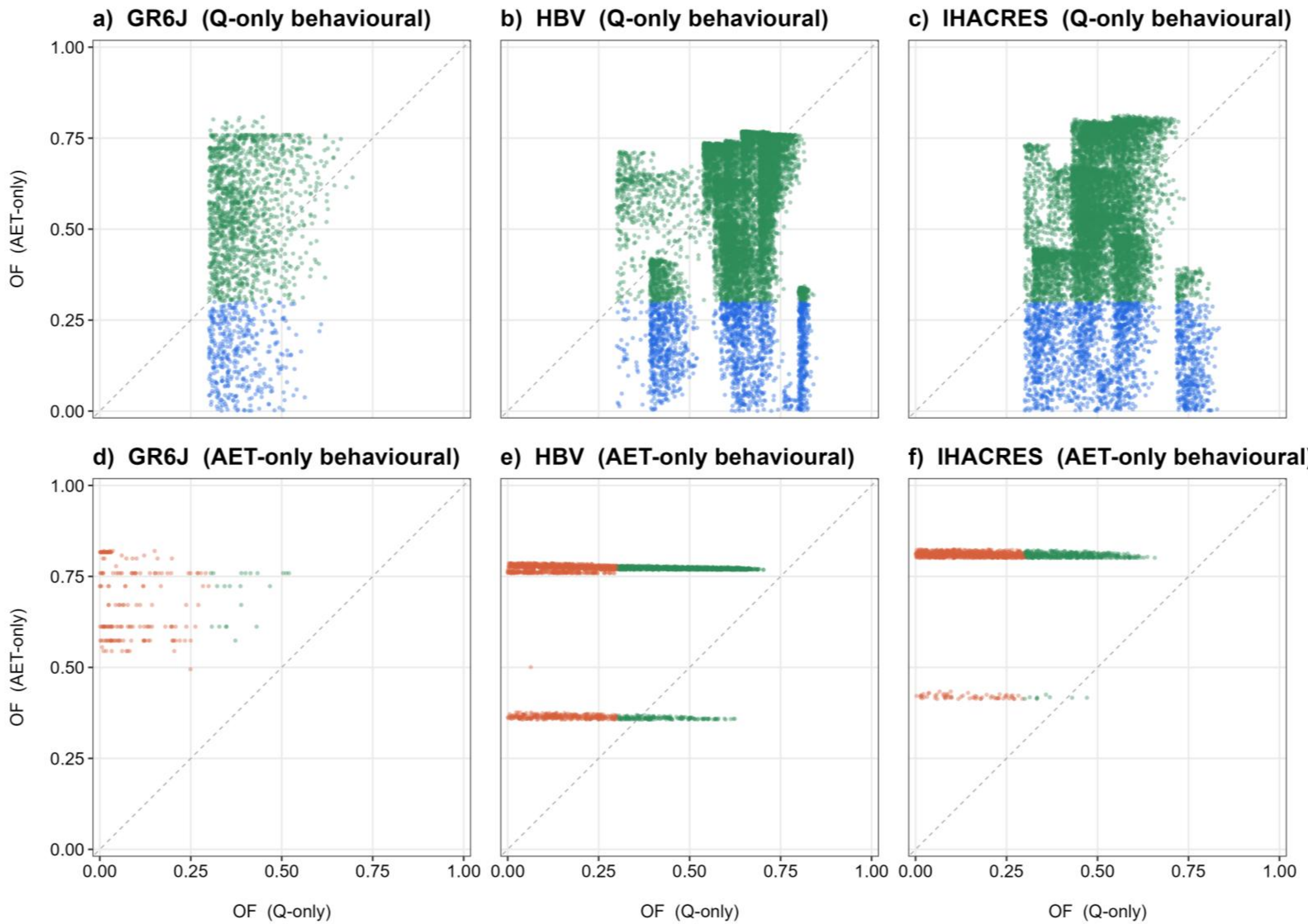

Figure S7: Joint behaviour of the Q and AET objective functions (OF_Q, OF_{AET}) across the 250,000-member prior sample, for GR6J, HBV and
45 **IHACRES (columns), pooling all 17 watersheds. (a-c) OF_{AET} plotted against OF_Q for parameter sets in the Q-only behavioural set (OF_Q > 0.3); green points also satisfy OF_{AET} > 0.3 (jointly behavioural), blue points do not. (d-f) OF_Q plotted against OF_{AET} for parameter sets in the AET-only behavioural set (OF_{AET} > 0.3); green points also satisfy OF_Q > 0.3, orange points do not. The dashed diagonal marks $OF_Q = OF_{AET}$. Departure from the diagonal, and the absence of a positive association between the two objective functions within each behavioural set, indicates that good performance on one flux does not imply good performance on the other.**

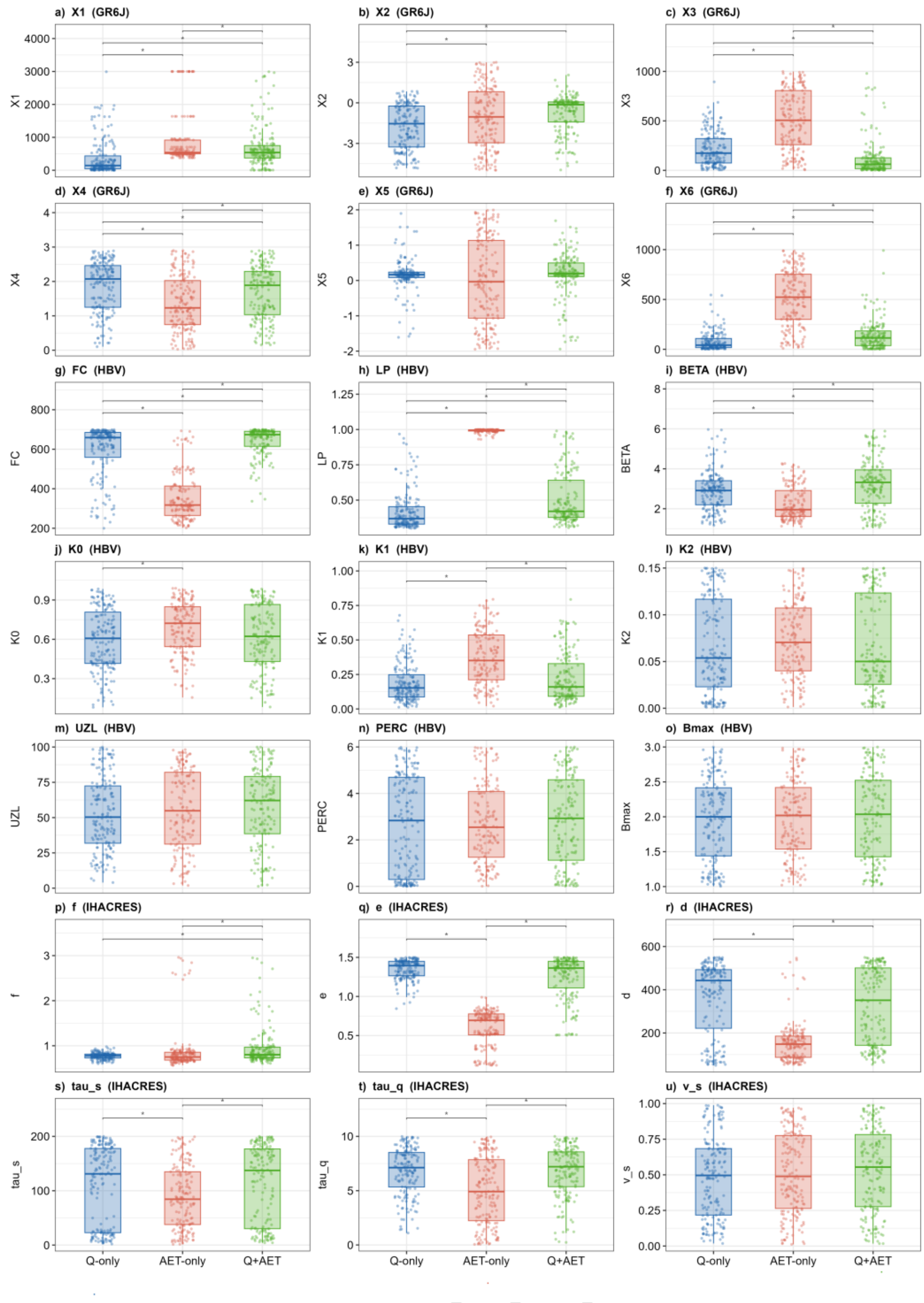

Figure S8: Behavioural (posterior) parameter values under the three calibration schemes, pooled across the 17 watersheds, for all parameters of (a-f) GR6J, (g-o) HBV and (p-u) IHACRES. Asterisks denote pairwise significant differences between schemes at the 5 % level.

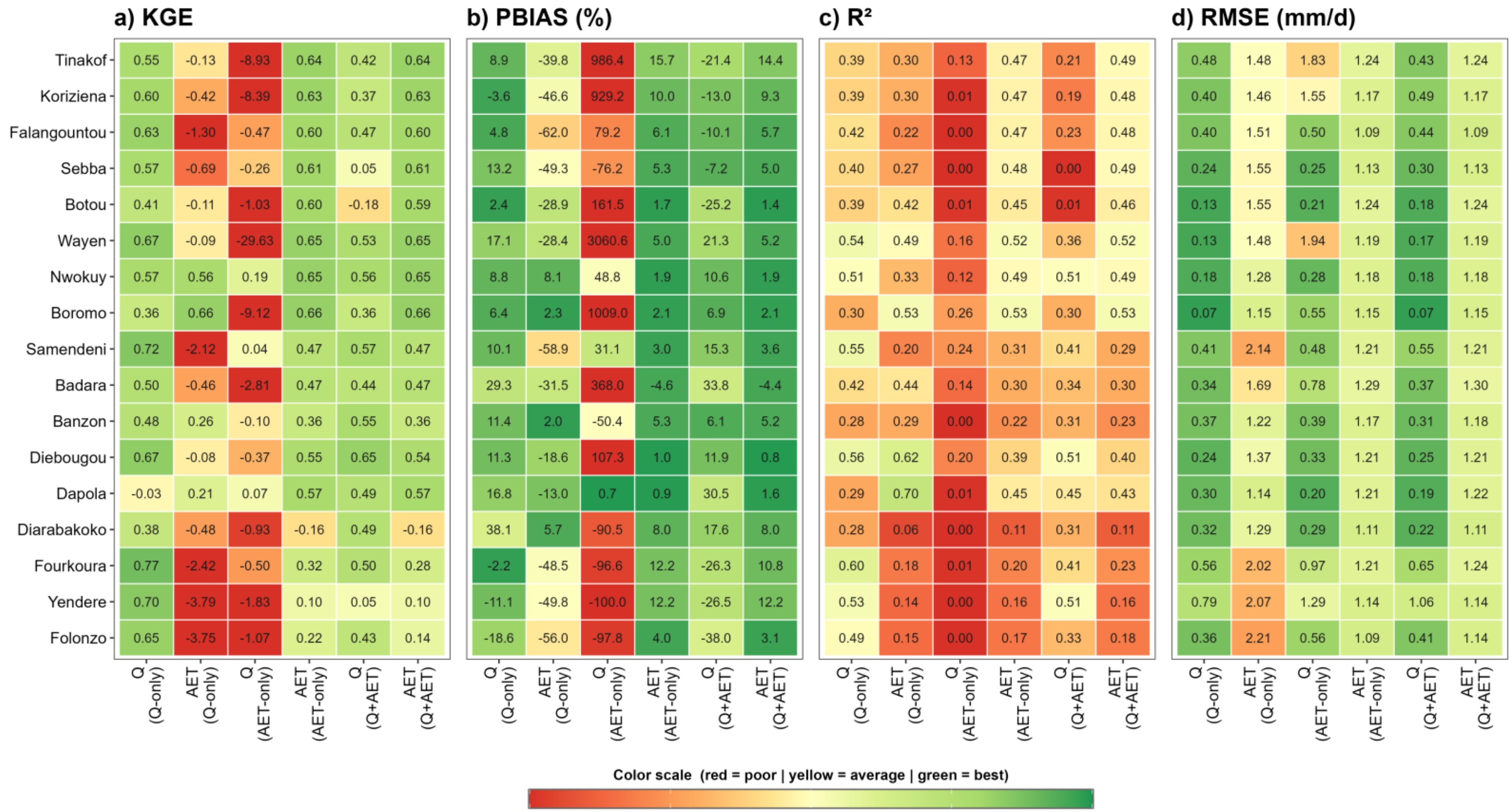

Figure S9: Per-watershed performance metrics (KGE, PBIAS, R², RMSE) for GR6J, comparing streamflow (Q) and AET simulations under each calibration scheme SCE-UA optimum (Q-only, AET-only, Q+AET). Colour scale is scaled independently per metric.

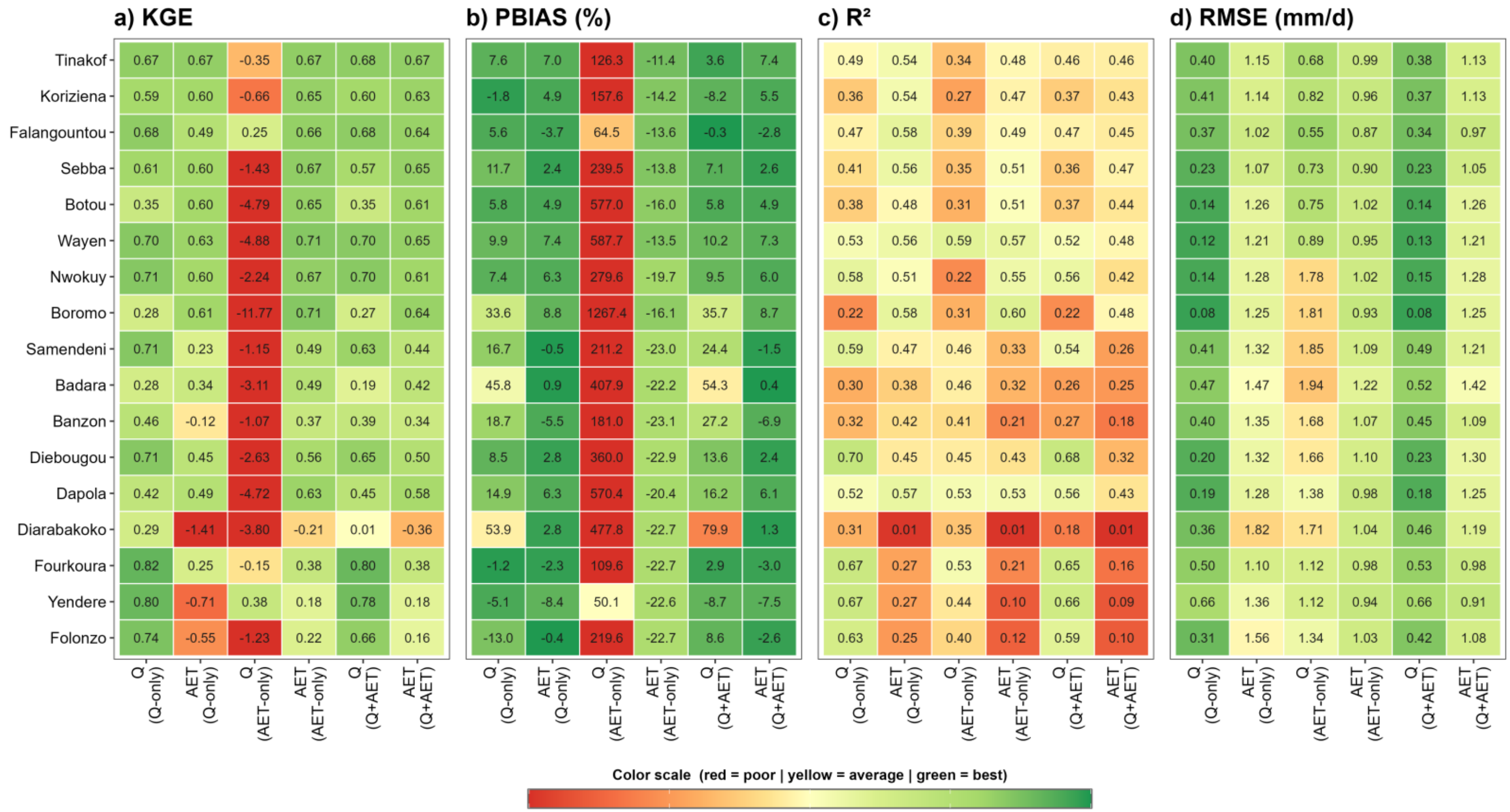

Figure S10: Per-watershed performance metrics (KGE, PBIAS, R², RMSE) for HBV, comparing streamflow (Q) and AET simulations under each calibration scheme SCE-UA optimum (Q-only, AET-only, Q+AET). Colour scale is scaled independently per metric.

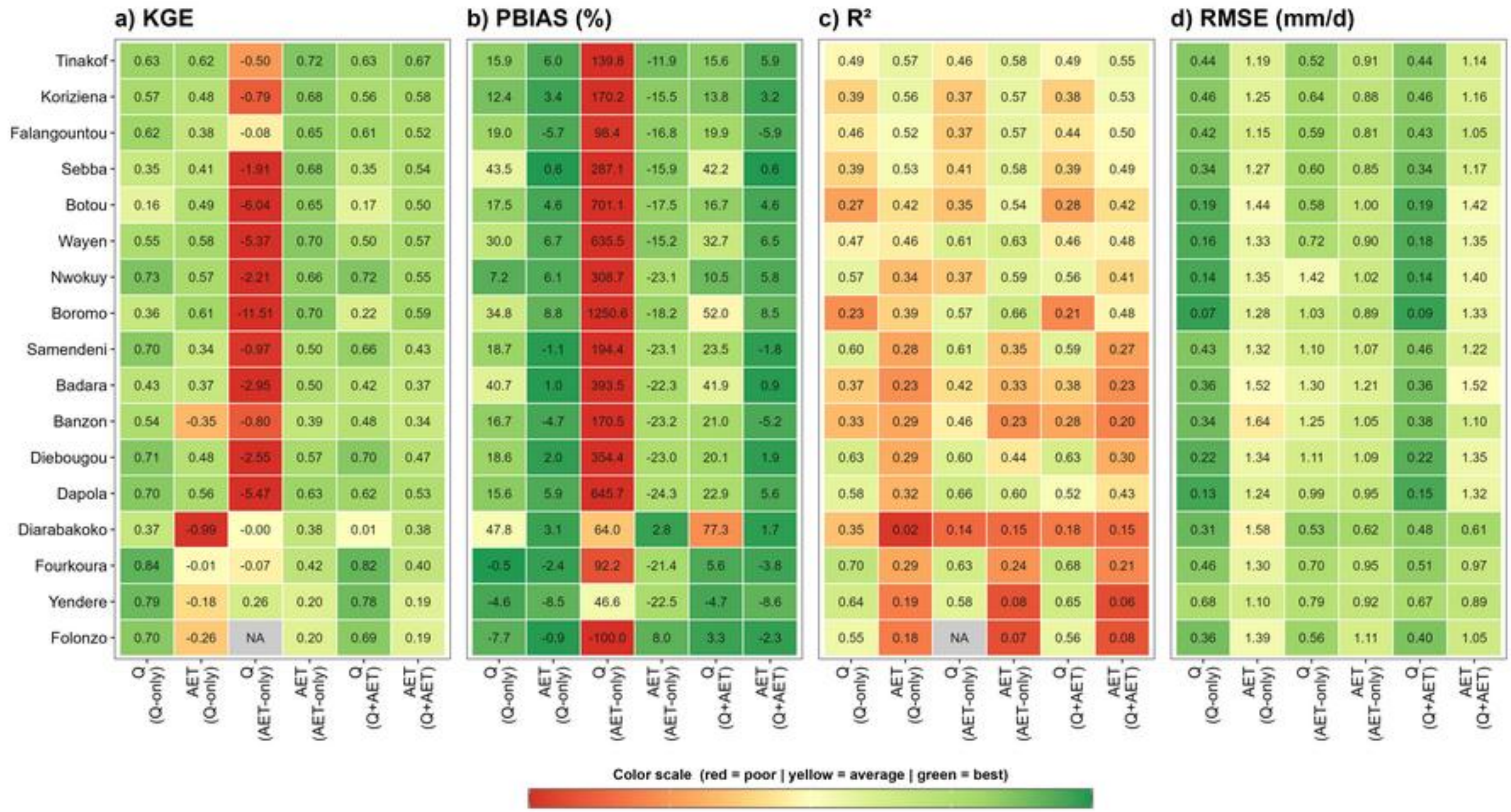

Figure S11: Per-watershed performance metrics (KGE, PBIAS, R², RMSE) for IHACRES, comparing streamflow (Q) and AET simulations under each calibration scheme SCE-UA optimum (Q-only, AET-only, Q+AET). Colour scale is scaled independently per metric.

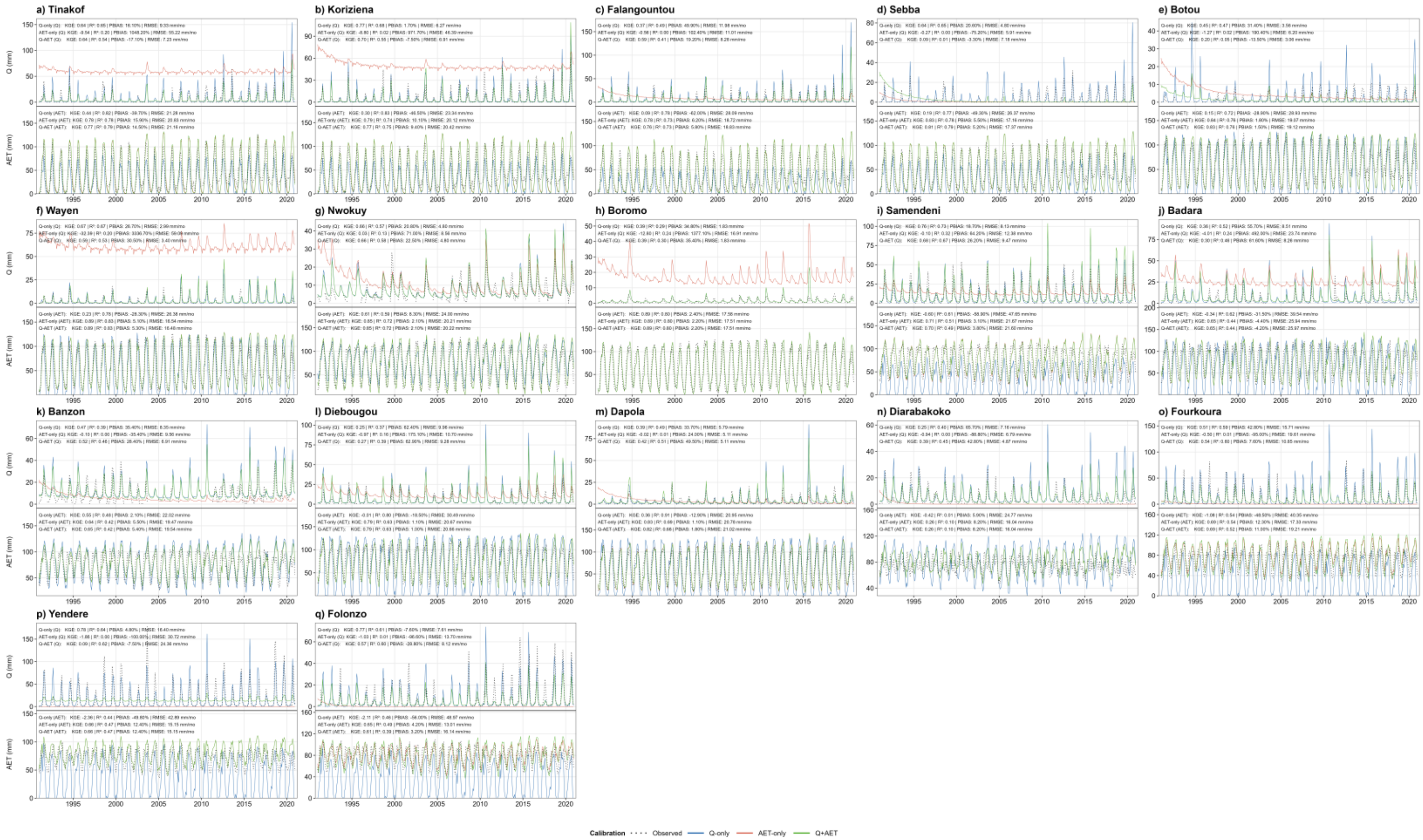

Figure S12: Monthly streamflow (upper sub-panel) and AET (lower sub-panel) timeseries simulated by GR6J under the three calibration schemes, compared with observations, for each of the 17 watersheds (a-q), 1991-2020. Inset text gives KGE, R², PBIAS and RMSE for each scheme-flux combination. Watersheds are ordered from north (a) to South (q).

Figure S13: Monthly streamflow (upper sub-panel) and AET (lower sub-panel) timeseries simulated by HBV under the three calibration schemes, compared with observations, for each of the 17 watersheds (a-q), 1991-2020. Inset text gives KGE, R², PBIAS and RMSE for each scheme-flux combination. Watersheds are ordered from north (a) to South (q).

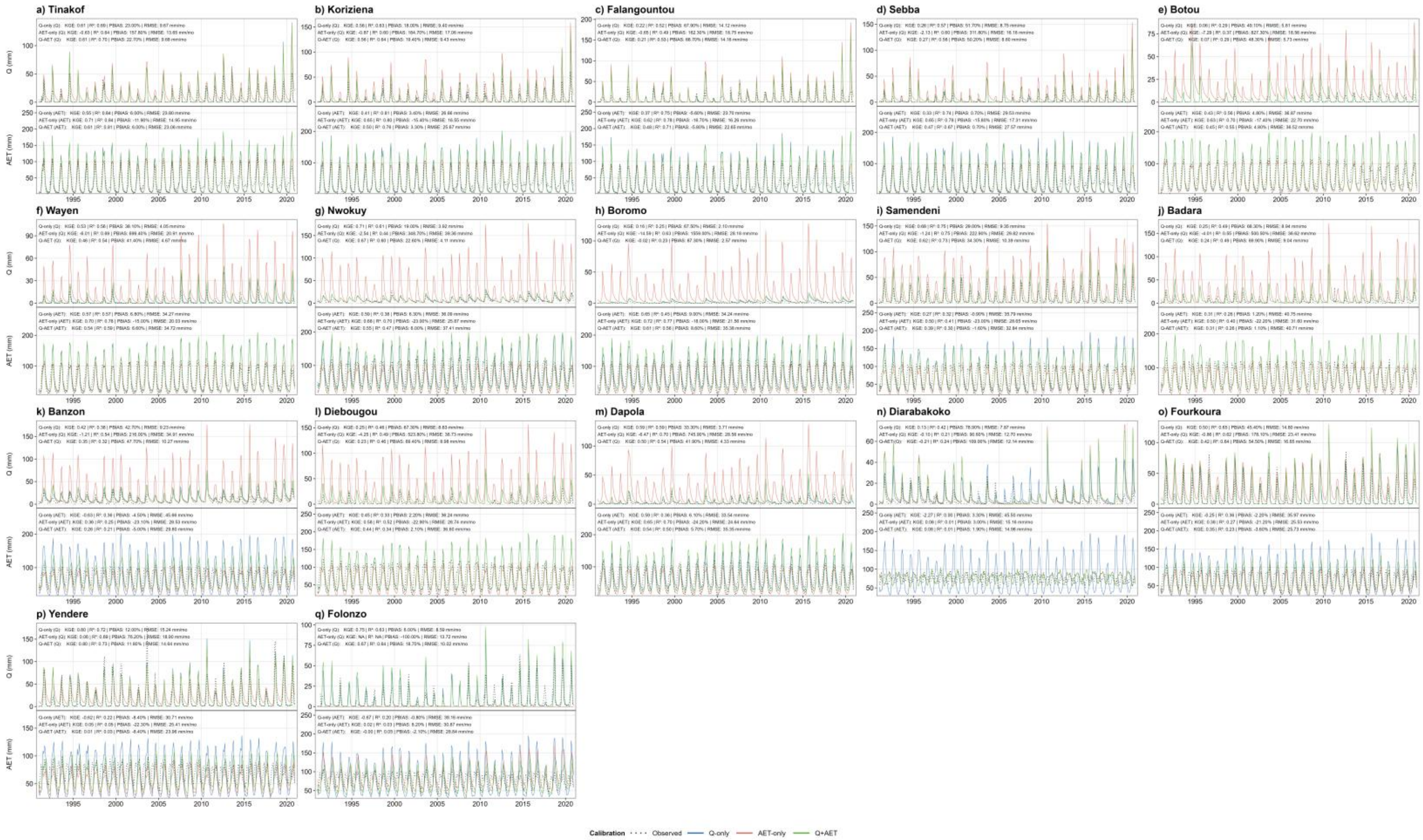

Figure S14: Monthly streamflow (upper sub-panel) and AET (lower sub-panel) timeseries simulated by IHACRES under the three calibration schemes, compared with observations, for each of the 17 watersheds (a-q), 1991-2020. Inset text gives KGE, R², PBIAS and RMSE for each scheme-flux combination. Watersheds are ordered from north (a) to South (q).

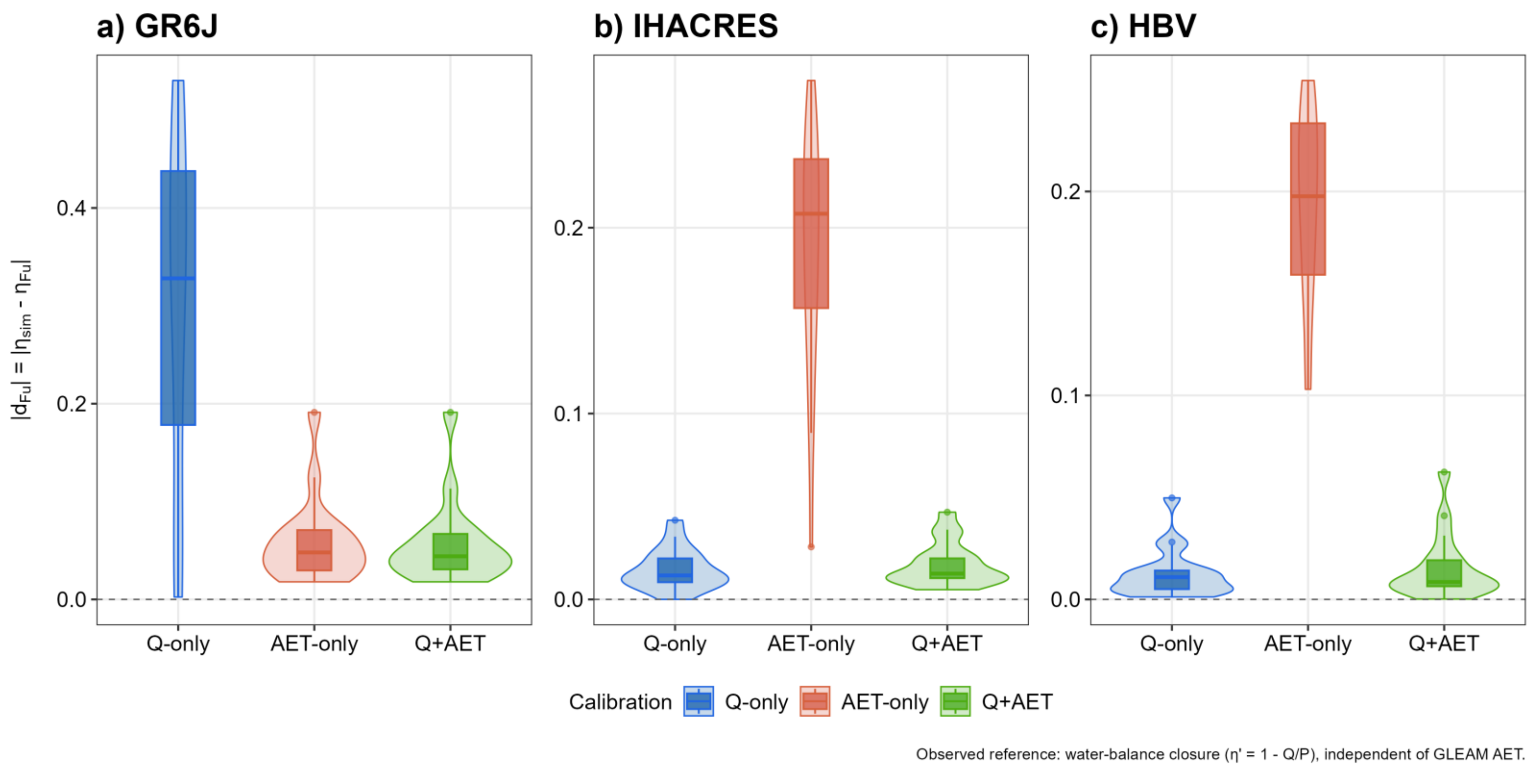

Figure S15: Absolute Budyko distance $|d_{Fu}|$ of the calibrated (SCE-UA) optima from the basin-specific Fu (1981) curve fitted on water-balance closure ($\eta' = 1 - Q/P$), by calibration scheme for (a) GR6J, (b) IHACRES and (c) HBV. Independent of GLEAM AET (compare with Fig. 13).

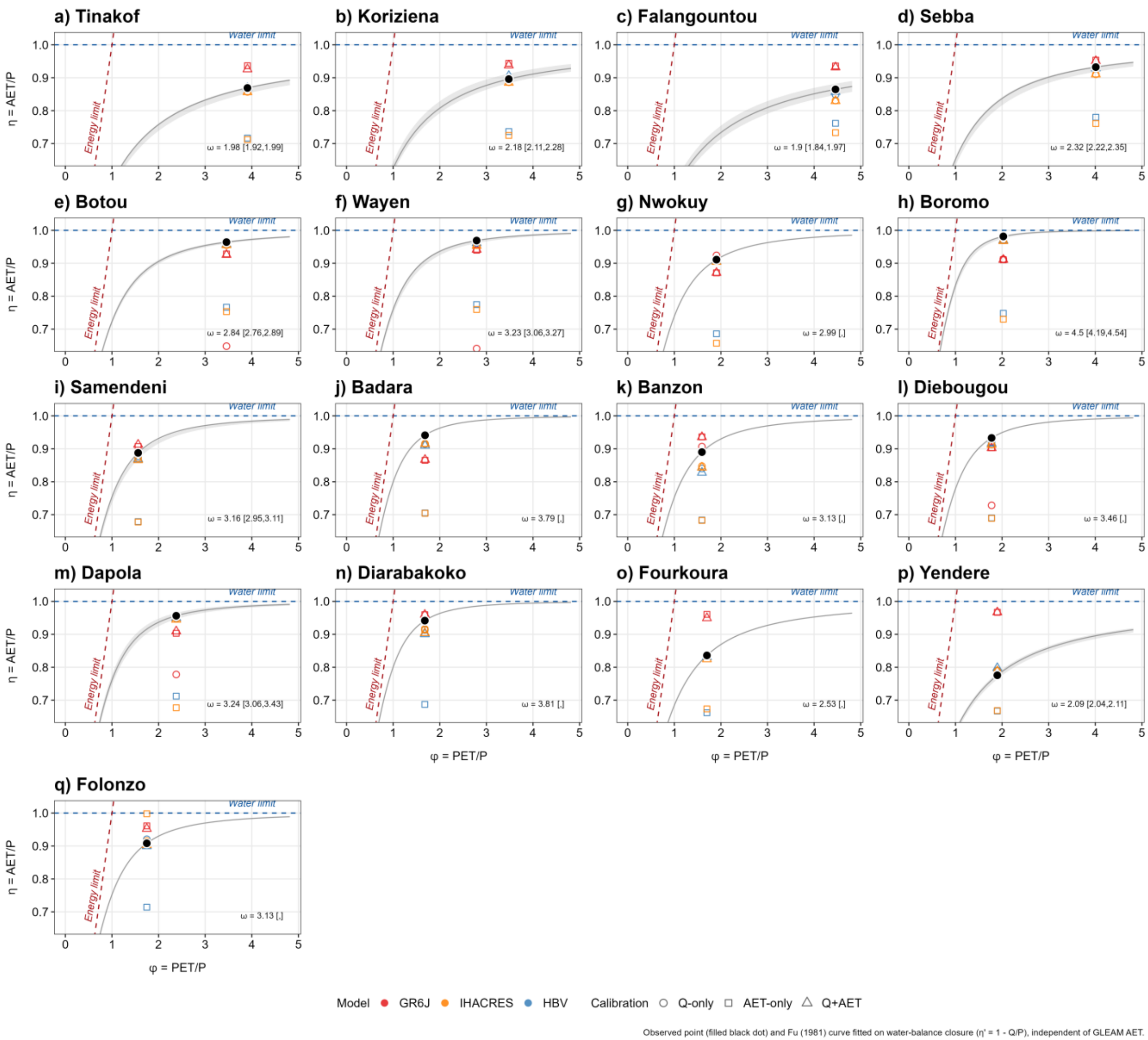

Figure S16: Position of the calibrated optima in Budyko space against the closure-based reference ($\eta' = 1 - Q/P$), for each of the 17 watersheds (a-q). The aridity index φ uses the joint P-PET-Q completeness mask required by the closure reference and slightly differs slightly from the φ values in Fig. 14, which use the P-PET-AET mask. The rolling-window ω uncertainty range could not be estimated for Nwokuy, Badara, Banzon, Diebougou, Diarabakoko, Fourkoura and Folonzo under this stricter mask (shown without brackets).

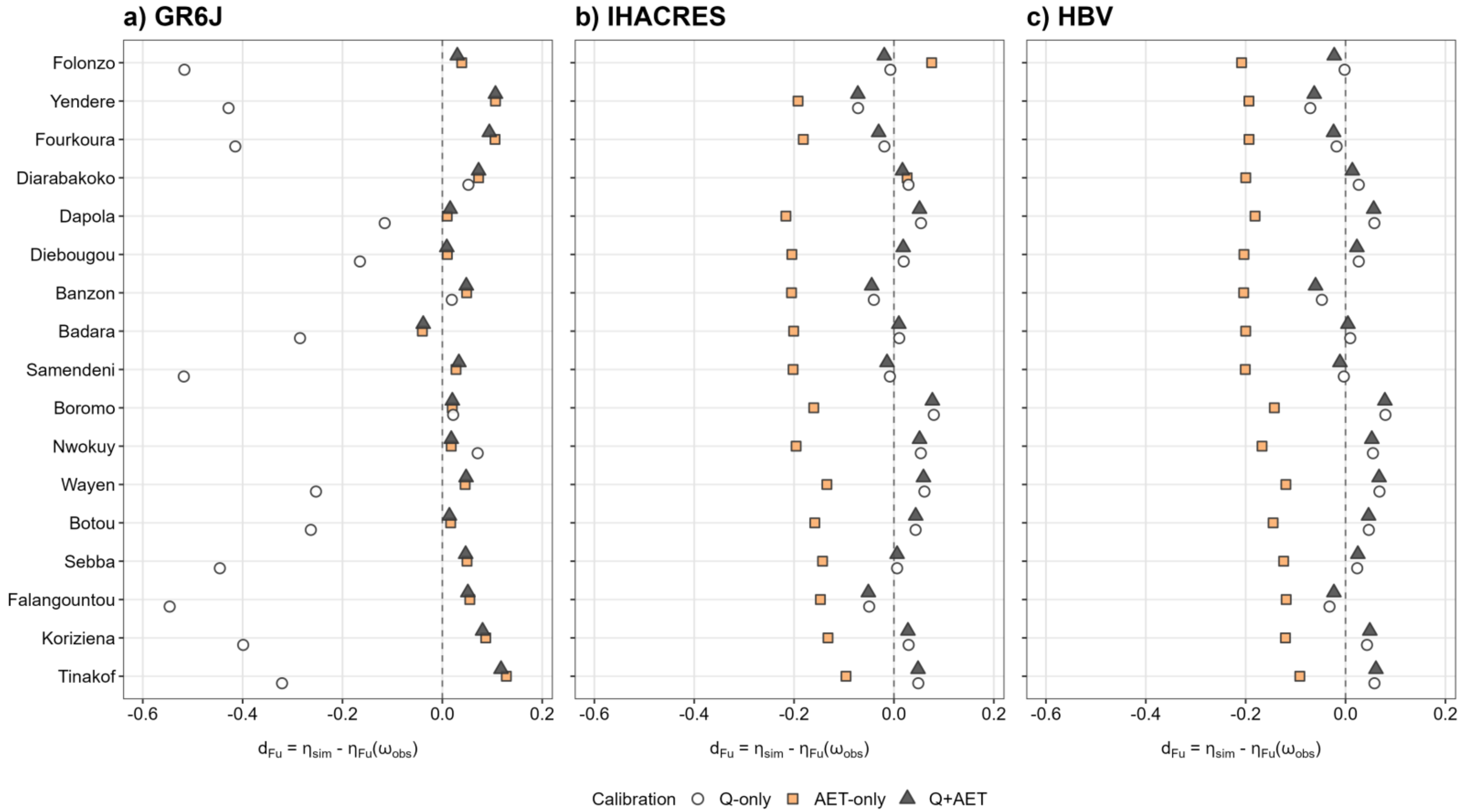

85 **Figure S17: Signed Budyko distance $d_{Fu} = \eta_{sim} - \eta_{Fu}(\varphi, \omega_{obs})$ per watershed (ordered north to south, bottom to top) for (a) GR6J, (b) IHACRES and (c) HBV, by calibration scheme. Negative values indicate underestimation of the evaporative index (and therefore overestimation of the runoff ratio).**

Table S1: Long-term mean annual water balance components for each of the 17 study watersheds over 1991-2020, ordered north to south.

Watershed	P (mm)	PET (mm)	Q (mm)	AET (mm)	dS (mm) / (dS/P)	Cr	EI	AI	EE
Tinakof	595.8	2190.3	75.1	481.5	39.2 (6.6%)	0.126	0.808	3.676	0.220
Koriziena	575.7	2172.1	56.7	493.3	25.6 (4.4%)	0.099	0.857	3.773	0.227
Falangountou	515.7	2135.6	59.7	454.1	1.9 (0.4%)	0.116	0.880	4.141	0.213
Sebba	584.6	2077.7	38	528.4	18.2 (3.1%)	0.065	0.904	3.554	0.254
Botou	782.1	2085	24.8	713	44.3 (5.7%)	0.032	0.912	2.666	0.342
Wayen	773.2	2019.6	21.1	691.2	60.9 (7.9%)	0.027	0.894	2.612	0.342
Nwokuy	1002	1932.3	91.6	854.9	55.6 (5.5%)	0.091	0.853	1.928	0.442
Boromo	846.4	1979.4	17.6	753.9	74.9 (8.8%)	0.021	0.891	2.338	0.381
Samendeni	1018.3	1860	106.8	895.7	15.8 (1.6%)	0.105	0.88	1.827	0.482
Badara	1049.8	1878	51.7	950.1	48 (4.6%)	0.049	0.905	1.789	0.506
Banzon	1012.1	1849.3	125	898.3	-11.3 (-1.1%)	0.124	0.888	1.827	0.486
Diebougou	1012.2	1883.4	66.2	904.2	41.8 (4.1%)	0.065	0.893	1.861	0.480
Dapola	848.8	1953.9	33.9	758.3	56.5 (6.7%)	0.040	0.893	2.302	0.388
Diarabakoko	1008.7	1792.6	44.3	894.7	69.7 (6.9%)	0.044	0.887	1.777	0.499
Fourkoura	977.2	1744.4	171.7	835.6	-30.1 (-3.1%)	0.176	0.855	1.785	0.479
Yendere	983.3	1763.9	199.8	846.1	-62.6 (-6.4%)	0.203	0.860	1.794	0.480
Folonzo	1009.2	1776.1	102	930.9	-23.7 (-2.3%)	0.101	0.922	1.760	0.524

$\boldsymbol{dS = P - AET - Q}$: long-term storage residual in mm, with the fractional residual $\boldsymbol{dS/P}$ in parentheses; $\boldsymbol{Cr = Q/P}$: runoff coefficient; $\boldsymbol{EI = AET/P}$: evaporative index ($\boldsymbol{\eta}$); $\boldsymbol{AI = PET/P}$: aridity index ($\boldsymbol{\varphi}$); $\boldsymbol{EE = AET/PET}$: evaporation efficiency. All values are area-averaged means computed from annual totals over the 30-year study period and used to verify approximate long-term water balance closure prior to the Budyko analysis.

References

Buiter, S.: How syn-rift sedimentation promotes the formation of hyper-extended margins, EGU General Assembly 2020, Online, 4–8 May 2020, EGU2020-18622, https://doi.org/10.5194/egusphere-egu2020-18622, 2020.

Loew, A., Bennartz, R., Fell, F., Lattanzio, A., Doutriaux-Boucher, M., and Schulz, J.: Surface Albedo Validation Sites, EUMETSAT [data set], https://doi.org/10.15770/EUM_SEC_CLM_1001, 2015.

Porter, J. G., De Bruyn, W., and Saltzman, E. S.: Eddy flux measurements of sulfur dioxide deposition to the sea surface, Atmos. Chem. Phys., 18, 15291–15305, https://doi.org/10.5194/acp-18-15291-2018, 2018.

Jung, M., Koirala, S., Weber, U., Ichii, K., Gans, F., Gustau-Camps-Valls, Papale, D., Schwalm, C., Tramontana, G., and Reichstein, M.: The FLUXCOM ensemble of global land-atmosphere energy fluxes, arXiv [preprint], arXiv:1812.04951, 11 December 2018.

Randall, D., Dazlich, D., Heikes, R., and Konor, C.: CSU model for DCMIP 2016, Zenodo [code], https://doi.org/10.5281/zenodo.5800992018, 2017.

Singh, O. N. and Fabian, P. (Eds.): Atmospheric Ozone: a Millennium Issue, Copernicus Publications, Katlenburg-Lindau, Germany, 147 pp., ISBN 393658608X, 2003.

van Edig, X., Schwarze, S., and Zeller, M.: The robustness of indicator based poverty assessment tools in changing environments – empirical evidence from Indonesia, in: Tropical Rainforests and Agroforests under Global Change, Environmental Science and Engineering (Environmental Engineering), edited by: Tscharntke, T., Leuschner, C., Veldkamp, E., Faust, H., Guhardja, E., and Bidin, A., Springer, Berlin, Heidelberg, Germany, 191–211, https://doi.org/10.1007/978-3-642-00493-3_9, 2010.